

Bayesian Optimization for Automatic Tuning of Torque-Level Nonlinear Model Predictive Control

Gabriele Fadini^{**}, Deepak Ingle^{*}, Tong Duy Son[†], Alisa Rupenyan^{*}

^{*} ZHAW Centre for Artificial Intelligence, Zürich University of Applied Sciences, Winterthur, Switzerland

[†] Siemens Digital Industries Software, Leuven, Belgium

Abstract—This paper presents an auto-tuning framework for torque-based Nonlinear Model Predictive Control (nMPC), where the MPC serves as a real-time controller for optimal joint torque commands. The MPC parameters, including cost function weights and low-level controller gains, are optimized using high-dimensional Bayesian Optimization (BO) techniques, specifically Sparse Axis-Aligned Subspace (SAASBO) with a digital twin (DT) to achieve precise end-effector trajectory real-time tracking on an UR10e robot arm. The simulation model allows efficient exploration of the high-dimensional parameter space, and it ensures safe transfer to hardware. Our simulation results demonstrate significant improvements in tracking performance (+41.9%) and reduction in solve times (-2.5%) compared to manually-tuned parameters. Moreover, experimental validation on the real robot follows the trend (with a +25.8% improvement), emphasizing the importance of digital twin-enabled automated parameter optimization for robotic operations.

Index Terms—Torque Control, Nonlinear Model Predictive Control, Trajectory Tracking, Real-Time Control, Bayesian Optimization, Robot Control, Digital Twin.

I. INTRODUCTION

Torque-based Model Predictive Control (MPC) has emerged as a powerful framework for robot control, enabling the direct selection of joint torques while planning optimal control sequences over a receding horizon [1]. Unlike kinematic controllers that rely on cascaded control loops, torque MPC computes optimal torque commands respecting actuator limits and dynamic constraints [2–4].

The practical success of torque MPC depends critically on tuning its many parameters, such as the weights in the optimization problem, solver tolerances, and the low-level controller feedback gains. Each combination creates different trade-offs between tracking accuracy, computational efficiency, and robustness. While MPC provides a solid foundation for optimal control, realizing its full potential requires systematic refinement of these parameters [5]. Manual tuning of this high-dimensional space is tedious, often suboptimal, and highly task-dependent. Unlike kinematic control, torque-level MPC enables higher compliance, making it suitable for contact-rich tasks and impedance control [6], but this formulation can potentially increase complexity and the chance of

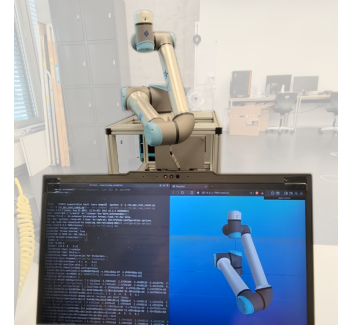


Fig. 1: UR10e robot executing torque-based MPC leveraging a digital twin for real-time optimization.

system modeling error. Hence, torque-level MPC requires accurate dynamics modeling to ensure successful sim-to-real transfer [7]. We address this challenge by leveraging a system’s digital twin for safe MPC parameter exploration (Fig. 1), combined with automated tuning methods [8–10]. Recent advances in Bayesian Optimization (BO) provide promising avenues for automated parameter tuning [5, 11–13]. In particular, Sparse Axis-Aligned Subspace Bayesian Optimization (SAASBO) [14, 15] has shown remarkable performance in high-dimensional problems (hundreds of parameters) by exploiting low-dimensional structure, making it well-suited for robotic applications.

This paper’s contributions are the following:

- Implementation of a torque-level nMPC interfaced with an extensible digital twin of the UR10e robot arm.
- Automated parameter optimization framework using high-dimensional Bayesian Optimization to balance real-time execution and control performance.
- Comprehensive testing demonstrating improvement over baselines in simulation and the real system.

II. PROBLEM FORMULATION

A. Robot Dynamics

Building upon prior force control methodologies [16, 17], we augment the classical MPC formulation with an explicit model of the robot’s actuation dynamics. We consider a robot manipulator operating under torque control, where the control input $\mathbf{u} \in \mathbb{R}^{n_u}$ consists of joint torque commands and n_u is the number of joints. The state of the robot is represented by $\mathbf{x} = [\mathbf{q}; \mathbf{v}] \in \mathbb{R}^{n_q + n_v}$, where the joint

^{*} Corresponding Author

This work was supported as a part of NCCR Automation, a National Centre of Competence in Research, funded by the Swiss National Science Foundation (grant number 51NF40.225155).

{fadi, inge, rupn}@zhaw.ch, son.tong@siemens.com

positions $\mathbf{q} \in \mathbb{R}^{n_q}$ and velocities $\mathbf{v} \in \mathbb{R}^{n_v}$. The robot dynamics follow the standard manipulator equation:

$$\mathbf{M}(\mathbf{q})\dot{\mathbf{v}} + \mathbf{C}(\mathbf{q}, \mathbf{v})\mathbf{v} + \mathbf{g}(\mathbf{q}) = \mathbf{u}, \quad (1)$$

where $\mathbf{M}(\mathbf{q}) \in \mathbb{R}^{n_v \times n_v}$ is the joint inertia matrix, $\mathbf{C}(\mathbf{q}, \mathbf{v})$ represents Coriolis and centrifugal terms, $\mathbf{g}(\mathbf{q})$ is the gravity vector, and \mathbf{u} are the applied joint torques.

B. Model Predictive Control Solver Description

We formulate the torque-based MPC optimal control problem at each time step $t \in [0, N]$ with discretization Δt as:

$$\begin{aligned} \min_{\mathbf{u}_0, \dots, \mathbf{u}_{N-1}} \quad & \sum_{k=0}^{N-1} \ell_k(\mathbf{x}_k, \mathbf{u}_k) \Delta t + \ell_N(\mathbf{x}_N) \\ \text{s.t.} \quad & \mathbf{x}_{k+1} = f(\mathbf{x}_k, \mathbf{u}_k), \quad k = 0, \dots, N-1 \\ & \mathbf{x}_0 = \mathbf{x}(t), \end{aligned} \quad (2)$$

where $f(\mathbf{x}_k, \mathbf{u}_k)$ is an Euler integrator computing the next state enforcing the system acceleration computed from (1) and $\ell_k(\mathbf{x}_k, \mathbf{u}_k)$ are the cost components to minimize. The first control \mathbf{u}_0^* is applied, then the horizon shifts forward. In addition to the dynamics and cost in (2), for robotic systems, the MPC planner must generate feasible trajectories that achieve the desired motion while respecting actuator and state limits approximated with the linear bounds:

$$\begin{aligned} \mathbf{q}_{\min} &\leq \mathbf{q}(t) \leq \mathbf{q}_{\max} && \text{Joint positions} \\ \mathbf{v}_{\min} &\leq \mathbf{v}(t) \leq \mathbf{v}_{\max} && \text{Joint velocities} \\ \mathbf{u}_{\min} &\leq \mathbf{u}(t) \leq \mathbf{u}_{\max} && \text{Torques,} \end{aligned} \quad (3)$$

where $(\cdot)_{\min}$ and $(\cdot)_{\max}$ denote the allowable limits.

We solve (2) using Differential Dynamic Programming (DDP) [4, 18], which efficiently exploits the time-sparse structure of the optimal control problem (linear with the number of problem nodes $\mathcal{O}(N)$). Given nominal trajectories $(\bar{\mathbf{x}}_t, \bar{\mathbf{u}}_t)_{t=0}^N$, DDP iteratively constructs a local quadratic approximation and improves the control sequence via backward-forward passes. The backward pass computes second-order value function approximations, yielding feed-forward gains \mathbf{k}_t and feedback gains \mathbf{K}_t . The forward pass then applies the improved control guess in simulation, locally improving the trajectories of states and control inputs for the next backward pass. At convergence, a locally optimal solution is achieved. Among other variants of DDP, Crocodyl's Feasibility-driven DDP (FDDP) [4], enables real-time performance through the relaxation of the constraints (3) as penalties, Hessian Newton approximation, and warm-starting capabilities.

C. Motivation for Torque-Level Model Predictive Control

Traditional kinematic-based MPC operates at the position-velocity level, abstracting dynamics for faster computation, commanding joint positions and velocities, but limiting compliant manipulation and force control [6, 19]. Torque-based MPC directly optimizes joint torques as decision variables, enabling contact-rich tasks [4], compliant behavior [17], and direct actuator optimization [3]. However, incorporating full dynamics (and joint torques as decision variables) increases

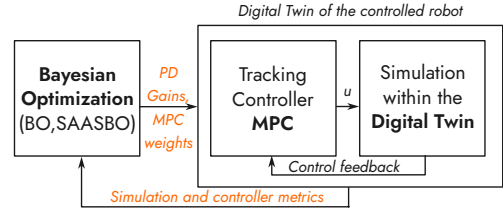


Fig. 2: Overview of the Bayesian Optimization, a digital twin is used to evaluate the MPC.

the computational complexity of the DDP problem from $\mathcal{O}((2n_q)^3 N)$ to $\mathcal{O}((3n_q)^3 N)$, requiring careful tuning of cost weights, solver tolerances, and feedback gains. This challenge lacks established heuristics, making systematic parameter optimization essential.

III. BAYESIAN OPTIMIZATION FRAMEWORK

A. Automatic Tuning Overview

Algorithm 1 presents our MPC hyperparameter auto-tuning framework. Our algorithm proceeds in two phases. First, an initial dataset is generated through Latin Hypercube sampling to uniformly explore the parameter space. For each sampled parameter vector θ_i , the MPC is executed in the digital twin, collecting the resulting trajectory data (\mathbf{x}, \mathbf{u}) and computing the objective function $J(\theta_i)$. This initial exploration phase produces n_0 observation pairs $\mathcal{D} = \{(\theta_i, y_i)\}_{i=1}^{n_0}$. Given such observations, a Gaussian process models the relationship between θ and y :

$$y \sim \mathcal{GP}(m(\theta), k(\theta, \theta')). \quad (4)$$

A Matérn-5/2 kernel is used, assuming J is twice differentiable:

$$k(\theta, \theta') = \sigma^2 \left(1 + \sqrt{5}r + \frac{5}{3}r^2 \right) \exp(-\sqrt{5}r), \quad (5)$$

where $r = \sqrt{\sum_{d=1}^D (\theta_d - \theta'_d)^2 / \ell_d^2}$ and ℓ_d are length scales learned via Markov Chain Monte Carlo (MCMC).

While in theory any Bayesian Optimization (BO) technique could be used in Algorithm 1, they would struggle with the curse of dimensionality. As a solution, we exploit SAASBO, which is particularly well-suited for high-dimensional tuning. SAASBO identifies a low-dimensional structure within the parameter space. Unlike standard BO, which treats all dimensions equally, SAASBO employs hierarchical sparsity-inducing priors (half-Cauchy distributions) on the inverse lengthscales of the GP kernel [20]. This encourages most parameters to have minimal influence while identifying a few critical dimensions, effectively reducing the search to a low-dimensional subspace. The method uses Hamiltonian Monte Carlo with No-U-Turn Sampler (NUTS) to identify these critical dimensions, offering three key advantages: (i) sample efficiency through selective modeling, (ii) preserved input geometry for better constraint handling, and (iii) robust scaling to hundreds of dimensions, making it ideal for the expensive MPC evaluations (each in the order of 10s).

Algorithm 1 MPC Parameters Optimization

```

1: Initialize hyperparameter bounds  $[\theta_{\min}, \theta_{\max}]$ 
2: Generate  $n_0$  Latin Hypercube samples
3: for  $i = 1$  to  $n_0$  do
4:   Run MPC with parameter  $\theta_i$  with digital twin
5:   Collect trajectory data  $\mathbf{x}, \mathbf{u}$ 
6:   Evaluate metric  $y_i = J(\theta_i)$ 
7: end for
8:  $\mathcal{D} \leftarrow \{(\theta_i, y_i)\}_{i=1}^{n_0}$ 
9: Initialize GP model based on  $\mathcal{D}$ 
10: for  $t = n_0 + 1$  to  $n_{\max}$  do
11:    $\theta_t \leftarrow \arg \max_{\theta} \text{EI}(\theta)$ 
12:   Evaluate metric  $y_t = J(\theta_t)$ 
13:    $\mathcal{D} \leftarrow \mathcal{D} \cup \{(\theta_t, y_t)\}$ 
14:   Refine GP model with  $\mathcal{D}$ 
15:   if no improvement for  $p$  iterations then
16:     Break (early stopping)
17:   end if
18: end for
19: return Optimal parameters:  $\theta^* = \arg \min_{\theta \in \mathcal{D}} J(\theta)$ 

```

At every iteration, the sparse \mathcal{GP} model identifies which regions of the reduced parameter space to explore. The Expected Improvement (EI) acquisition function is used:

$$\text{EI}(\theta) = \mathbb{E}[\max(f^* - f(\theta), 0)], \quad (6)$$

where f^* is the current best observed value. The next evaluation point chosen by maximizing the EI:

$$\theta_{n+1} = \arg \max_{\theta} \text{EI}(\theta). \quad (7)$$

At every iteration, a new observation is added to the dataset \mathcal{D} , refining the \mathcal{GP} . The optimization terminates when no improvement is observed over p consecutive iterations, or when a maximum iteration budget n_{\max} is reached. The best achieved parameter configuration θ^* during the optimization is finally selected.

IV. IMPLEMENTATION DETAILS

A. Digital Twin for Parameter Optimization

Each iteration of Algorithm 1 requires evaluating the MPC planner with different hyperparameters θ , as shown in Fig. 2. This can be sped up *in silico*, making automated optimization feasible. A digital twin of the UR10e robot, built using Pinocchio [21], with a parameterized URDF model, enables safe exploration of the MPC hyperparameter space. The digital twin also enables safe testing, avoiding failure modes (joint limits, actuator saturation) that would be dangerous on the physical system. The fidelity of the digital twin to the real robot is validated, after calibration of the end-effector. We verify that the kinematic position estimation of the end-effector matches, within numerical precision $\approx 10^{-16}$, the one estimated by the robot internal functions. Also, the values of the computed joint mass inertia matrix $\mathbf{M}(\mathbf{q})$ are compared to those obtained from the real robot for 100 random joint configurations, showing an average error of

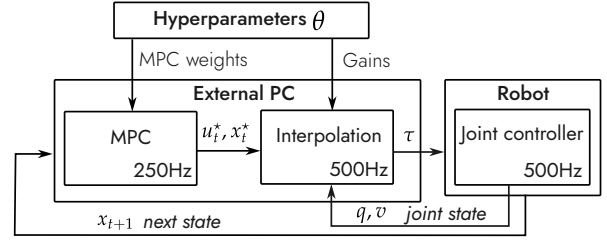


Fig. 3: Low-level torque control interface for UR10e robot using RTDE library.

$2 \cdot 10^{-5}$ (Frobenius norm). Our digital twin hence captures well kinematic and dynamic properties but, due to the lack of external sensors, we cannot encompass friction, backlash, or communication delays.

B. Low-Level Joint Controller

To bridge the real-time gap between the MPC frequency (125-250 Hz due to computational constraints) and the required 500 Hz robot control frequency, we employ joint-space and task-space feedback. At each MPC update, the solver provides an optimal torque trajectory $\{\mathbf{u}_0^*, \mathbf{u}_1^*, \dots, \mathbf{u}_{N-1}^*\}$ along with the associated optimal state trajectory $\{\mathbf{x}_0^*, \mathbf{x}_1^*, \dots, \mathbf{x}_{N-1}^*\}$. Between MPC updates, torque commands are interpolated at higher frequency, and corrected with joint and task feedback components:

$$\begin{aligned} \tilde{\mathbf{u}}(t) = & \mathbf{u}_k^* + \mathbf{K}_d(\mathbf{v}_{k+1}^* - \mathbf{v}(t)) + \mathbf{K}_p(\mathbf{q}_{k+1}^* - \mathbf{q}(t)) \\ & + \mathbf{K}_{p,c} \mathbf{J}_k^\top (\mathbf{p}(\mathbf{q}_{k+1}^*) - \mathbf{p}(\mathbf{q}(t))) \\ & + \mathbf{K}_{d,c} \mathbf{J}_k^\top (\mathbf{J}_{k+1}(\mathbf{v}_{k+1}^*) - \mathbf{J}_k(\mathbf{v}(t))), \end{aligned} \quad (8)$$

where, at every time step k , \mathbf{u}_k^* and \mathbf{v}_{k+1}^* are the optimal torque and velocity from the MPC solution, and $\mathbf{K}_p, \mathbf{K}_d \in \mathbb{R}$ are respectively joint position and velocity feedback gain. By computing $\mathbf{p}, \mathbf{v}, \mathbf{J}$, respectively, the end-effector's position velocities, and the joint Jacobian, we can also add a task-dependent feedback where $\mathbf{K}_{p,c}, \mathbf{K}_{d,c} \in \mathbb{R}^3$ are the cartesian position and velocity gains.

This hybrid feedback-feedforward controller structure is critical for real-world deployment to maintain more reliable tracking performance. This controller formulation strikes a balance between expressiveness, interpretability, and a reduced number of governing parameters, which is desirable for automated tuning.

The joint torque commands $\boldsymbol{\tau}$ computed after interpolation are executed on the UR10e robot using the direct torque control API introduced in the UR10e firmware and the RTDE 1.6.2 library [22]. This interface provides low-level access to joint-level torque control [23]. The UR10e torque controller additionally compensates for gravity forces $\mathbf{g}(\mathbf{q})$ acting on the robot as in (1). The command sent to the robot, to enforce safety, is additionally saturated and compensated:

$$\boldsymbol{\tau} = \text{sat}(\tilde{\mathbf{u}}, \mathbf{u}_{\min}, \mathbf{u}_{\max}) - \mathbf{g}(\mathbf{q}), \quad (9)$$

where $\text{sat}(\cdot, \mathbf{u}_{\min}, \mathbf{u}_{\max})$ denotes element-wise saturation to ensure commanded torques remain within the actuator limits.

TABLE I: Model Predictive Control Cost Weights

Cost Components	Default	Optimized	
<i>Running Costs Weights</i>			
Position tracking, w_{pos}	10^5	Vanilla BO 7.2×10^4	SAASBO 4.1×10^4
Rotation tracking, w_{rot}	10^{-4}	5.8×10^{-5}	2.3×10^{-5}
Control reg., w_{τ}	10^{-2}	6.5×10^{-3}	3.7×10^{-3}
Joint velocities, w_v	10^{-3}	8.1×10^{-4}	7.9×10^{-4}
<i>Fixed Running Cost Weights</i>			
Control limits, $w_{\text{lim},\tau}$	10^1	10^1	10^1
Joint limits, $w_{\text{lim},x}$	10^1	10^1	10^1
<i>Terminal Cost Weight</i>			
Position tracking, $w_{\text{pos},N}$	w_{pos}	w_{pos}	w_{pos}

C. MPC Formulation

Tracking Task: The control objective is to track a reference end-effector trajectory $\mathbf{p}_{\text{des}}(t)$ while minimizing tracking error, control effort, and joint limits. We generate trajectories (square, hexagon, circle) with parameterized size and center as in Fig. 4, with reference point $\mathbf{p}_{\text{des}}(t)$ and end-effector orientation $\mathbf{R}_{\text{des}}(t)$ being linearly interpolated between vertices based on a task-progress variable $\phi \in [0, 1]$.

Omitting the time index k , at every node, the running cost $\ell(\mathbf{x}, \mathbf{u})$ takes the form:

$$\begin{aligned} \ell(\mathbf{x}, \mathbf{u}) = & w_{\text{pos}} \|\mathbf{p}(\mathbf{q}) - \mathbf{p}_{\text{des}}\|^2 + w_{\text{rot}} \|\mathbf{R}(\mathbf{q}) - \mathbf{R}_{\text{des}}\|_F^2 + \\ & w_{\tau} \|\mathbf{u}\|^2 + w_v \|\mathbf{v}\|^2 + \\ & w_{\text{lim},\tau} \Gamma(\mathbf{u}) + w_{\text{lim},x} \Gamma(\mathbf{x}), \end{aligned} \quad (10)$$

where \mathbf{p} and \mathbf{R} represent the end-effector position and orientation, $\Gamma(\mathbf{u})$ and $\Gamma(\mathbf{x})$ are quadratic barrier functions enforcing control and actuator limits (velocity and position), and w_{\cdot} are tunable MPC weights that determine the trade-off between tracking accuracy, control smoothness, and constraint satisfaction. The terminal cost adds $w_{\text{pos},N} \|\mathbf{p}(\mathbf{q}_N) - \mathbf{p}_{\text{des},N}\|^2$ at the horizon end N , with $w_{\text{pos},N}$ coupled to w_{pos} to maintain consistency between running and terminal objectives. Table I summarizes the nominal cost weights used in the MPC formulation.

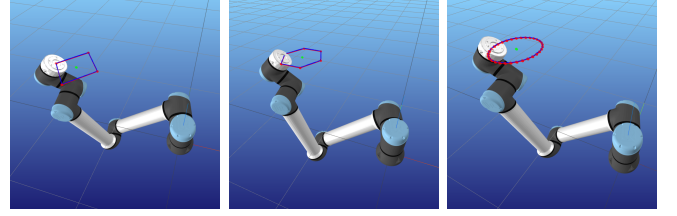
All cost weights except the barrier-dependent ones are tunable hyperparameters for optimization. In the decision variables $\boldsymbol{\theta} \in \mathbb{R}^{12}$ we also include the joint and task gains:

$$\boldsymbol{\theta} = [w_{\text{pos}}, w_{\text{rot}}, w_{\tau}, w_v, \mathbf{K}_p, \mathbf{K}_d, \mathbf{K}_{p,c}, \mathbf{K}_{d,c}], \quad (11)$$

where the different terms have been defined in (8) and (10). The objective function balances optimality with real-time performance with a convex combination depending on a tunable parameter $\alpha \in [0, 1]$:

$$J(\boldsymbol{\theta}) = \alpha \cdot \mathcal{L} + (1 - \alpha) \cdot t_{\text{solve}}, \quad (12)$$

where \mathcal{L} is the accumulated cost over the trajectory as in (2), and t_{solve} is the average DDP solve time. In our experiments, we set $\alpha = 0.8$ to prioritize tracking performance. The optimization seeks parameters that enable the MPC to generate torques, achieving minimal tracking error while ensuring the DDP solver converges within real-time constraints.



(a) Square (b) Hexagon (c) Circle

Fig. 4: Tracking MPC trajectories in task-space.

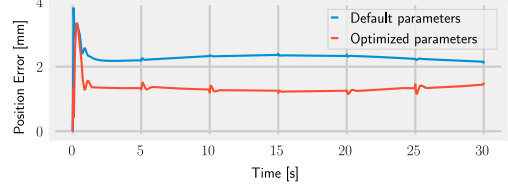


Fig. 5: Tracking error trend, the baseline is compared with optimized parameters.

1) Solver Configuration and Real-Time Control: The reactive controller MPC employs FDDP from Crocoddyl [4] with a horizon of $N = 20$ steps (50ms lookahead), maximum 10 iterations per solver call, targeting $\leq 2\text{ms}$ solve time for 500 Hz control. At every cycle the solver is warm-started from previous solutions.

D. High-dimensional Bayesian Optimization Configuration

For the SAASBO optimization, we configure the following settings and implement the algorithm using the BoTorch library [24] and AX platform [25]. The optimization begins with $n_0 = 100$ initial samples generated via Latin Hypercube sampling to ensure uniform coverage of the 12-dimensional parameter space, followed by 200 Bayesian Optimization iterations. Each MPC evaluation requires $\approx 15\text{--}20$ s in the digital twin, making the total parameter tuning feasible in 1h06min. The early stopping threshold $p = 10^2$ ensures thorough exploration improving the \mathcal{GP} model, though convergence typically occurs earlier. The Gaussian process hyperparameters are inferred using MCMC with 1024 warmup steps and 1024 posterior samples (thinned by 16) for robust uncertainty quantification. The kernel uses smoothness $\nu = 2.5$ with output scale σ^2 and lengthscales ℓ_d learned via MCMC, while a fixed noise variance 10^{-6} reflects the near-deterministic simulation.

V. EXPERIMENTAL RESULTS

A. Automatic Tuning Results in Simulation

We run the optimization loop (Algorithm 1), evaluating the MPC planner on the digital twin for each sampled parameter set in a task in which the UR10e robot tracks a hexagonal trajectory (Fig. 4) of 10cm side length in a total time of 30 s. The optimization yields a set of parameters that significantly improves tracking performance, while it maintains reliable real-time control performance, compared

TABLE II: Trajectory End-effector Tracking in Simulation

Method	Avg Error (mm)	Max Error (mm)
Baseline	2.29 ± 0.15	3.81
Vanilla BO	1.61 ± 0.18	3.57
SAASBO	1.33 ± 0.22	3.33
Improvement (Vanilla BO)	+29.7%	+6.3%
Improvement (SAASBO)	+41.9%	+12.5%

TABLE III: Optimized Feedback Gains

Control Level	Gain	Default	Vanilla BO	SAASBO
Joint-space	\mathbf{K}_p	1	12.3	28.7
Joint-space	\mathbf{K}_d	1	0.45	0.18
Task-space	$\mathbf{K}_{p,c}$	[1, 1, 1]	[3.2, 2.8, 15.4]	[7.8, 6.5, 89.2]
Task-space	$\mathbf{K}_{d,c}$	[1, 1, 1]	[1.5, 1.3, 8.7]	[2.1, 1.8, 10.3]

to both the manually adjusted default baseline and a vanilla BO approach using the same seed, configuration, and initial population as described in Section IV-D.

1) *Weights Analysis*: Fig. 5 illustrates the reduction in tracking error over the optimization process. Table II presents the tracking performance comparison. Tab. I compares the cost weights across methods, with the SAASBO column showing the most effective configuration. The position tracking weight w_{pos} is reduced by an order of magnitude, indicating that overly aggressive tracking can lead to instability or excessive control effort. The control regularization weight w_{τ} is also decreased, allowing for more responsive torque commands. The rotation tracking weight w_{rot} is lowered, suggesting that precise orientation tracking is less critical for the task. Additionally, with optimized weights, the MPC solver achieves a modest 2.55% reduction in the average number of DDP iterations (on average 1.009 iterations in 2 ms), enabling consistent real-time execution.

2) *Gain Analysis*: The trade-off between feedforward MPC torque and feedback terms is non-trivial, and understanding optimal gain magnitudes while avoiding instability is aided by the use of the digital twin to predict performance. The optimized hybrid controller increases the feedback contribution for tracking. Table III summarizes the gains used for the controller. Joint stiffness increases significantly while damping decreases, suggesting the system benefits from aggressive proportional tracking with minimal derivative action. Task-space gains show substantial increases in the z-axis (vertical): compared to xy-plane values, reflecting the need for higher vertical stiffness for a precise lateral motion execution.

3) *Comparison with Vanilla Bayesian Optimization*: Starting from the same priors and an initial cost of 2.677, SAASBO achieves a final cost of 0.23 after 200 iterations (91.3% improvement), while vanilla BO reaches 0.703 (29.7% improvement). This substantial gap arises because vanilla BO treats all 12 parameters equally, spreading its modeling capacity across the full space. In contrast, SAASBO's sparsity-inducing priors effectively identify that only 3-5 parameters dominate performance (primarily w_{pos} ,

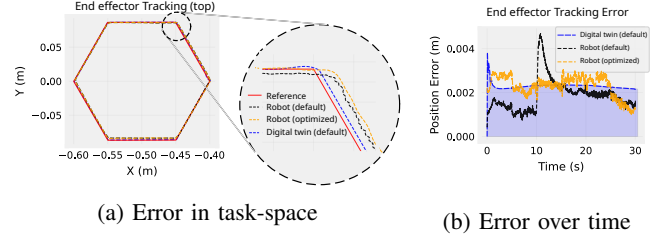
Fig. 6: Comparison of the optimization progress (best cost from parameters θ^*) between SAASBO and vanilla BO.

Fig. 7: End-effector cartesian tracking error in simulation and on the robot for the hexagon trajectory.

\mathbf{K}_p , and z-axis task gains), enabling focused exploration of the relevant subspace and reducing the effect of the curse of dimensionality. In Fig. 6, the trend of the current best cost value over iterations is shown for both methods, highlighting how SAASBO consistently improves throughout the optimization, while vanilla BO returns a worse solution within the computation constraints.

B. Experimental testing on the real robot

Hardware validation of parameters found in Sec. V-A was conducted on the UR10e robot tracking the same hexagonal trajectory as in Sec. V-A. Fig. 7 shows the tracking performance across three configurations: default parameters in the digital twin (blue), default parameters on the real robot (black), and optimized parameters on the real robot (yellow). Fig. 7a shows the Cartesian tracking error in task space. The optimized parameters produce trajectories (yellow) that remain generally closer to the reference path (red) and exhibit fewer high-frequency oscillations compared to the ones from default parameters (black). The results show an increase in tracking error for both default and optimized parameters when transferring from simulation to hardware, likely due to unmodelled effects such as friction, communication delays, and sensor noise.

The position tracking error in time, shown in Fig. 7b, shows that the parameters optimized with SAASBO achieve a lower average tracking error (yellow) and significantly reduced error peaks compared to the default ones (black). Quantitatively, the average tracking error on hardware is 2.3 mm for the SAASBO optimized parameters versus the 3.1 mm achieved with the default parameters (25.8% improvement). The relative improvement from optimization (25.8% on hardware vs. 41.9% in simulation) shows that the optimal parameters translate to the system, validating the digital twin as an effective optimization surrogate for real experimentation despite the sim-to-real gap.

VI. CONCLUSION AND FUTURE WORK

We demonstrate that systematic hyperparameter optimization is beneficial to tune torque-based nMPC in robotic trajectory tracking tasks. For this, an automated tuning framework was introduced, combining high-dimensional Bayesian Optimization (SAASBO) with a digital twin to efficiently explore the MPC parameters before hardware deployment. Our results explore torque-level nMPC coupled with reactive feedback. We, moreover, demonstrate the importance of sparsity-inducing priors for high-dimensional optimization in robotic applications showing that vanilla BO stagnates in finding the best configuration. The sim-to-real transfer in Sec. V-B validates the effectiveness of our method and the digital twin as surrogate. Our experimental validation shows that 41.9% tracking improvement (compared to a baseline) in simulation still translates to a 25.8% improvement on hardware. Further modeling of friction, delays, and sensor noise could further reduce the current sim-to-real gap [12]. To this end, our digital twin could either encompass a more detailed multi-domain physical simulation or incorporate a data-driven approach. Despite our results showing promise for parameter automatic tuning, the method may still struggle in high-dimensional settings. We hence plan further validation of the method for other complex tasks, where parameter sensitivity is more pronounced, such as contact-rich manipulation.

REFERENCES

- [1] James Blake Rawlings, David Q. Mayne, and Moritz Diehl. *Model predictive control: theory, computation, and design*. Madison, Wisconsin: Nob Hill Publishing, 2017.
- [2] Rohan Budhiraja et al. “Differential Dynamic Programming for Multi-Phase Rigid Contact Dynamics”. In: *2018 IEEE-RAS 18th International Conference on Humanoid Robots (Humanoids)*. 2018, pp. 1–9.
- [3] Yuval Tassa, Nicolas Mansard, and Emo Todorov. “Control-limited differential dynamic programming”. In: *Proceedings - IEEE International Conference on Robotics and Automation*. 2014.
- [4] Carlos Mastalli et al. “Crocodyl: An Efficient and Versatile Framework for Multi-Contact Optimal Control”. In: *IEEE Int. Conf. on Robotics & Automation*. 2020.
- [5] Alisa Rupenyan, Mohammad Khosravi, and John Lygeros. “Performance-based Trajectory Optimization for Path Following Control Using Bayesian Optimization”. In: *2021 60th IEEE Conference on Decision and Control (CDC)*. 2021.
- [6] Neville Hogan. “Impedance Control: An Approach to Manipulation: Part I—Theory”. In: *Journal of Dynamic Systems, Measurement, and Control* 107.1 (Mar. 1985), pp. 1–7.
- [7] Côme Perrot and Olivier Stasse. “Step Toward Deploying the Torque-Controlled Robot TALOS on Industrial Operations”. In: *2023 IEEE/RSJ International Conference on Intelligent Robots and Systems (IROS)*. 2023 IEEE/RSJ International Conference on Intelligent Robots and Systems (IROS). Detroit, MI, USA: IEEE, Oct. 1, 2023, pp. 10405–10411.
- [8] William Edwards et al. “Automatic Tuning for Data-driven Model Predictive Control”. In: *2021 IEEE International Conference on Robotics and Automation (ICRA)*.
- [9] Albert Gassol Puigjaner et al. “Performance-Driven Constrained Optimal Auto-Tuner for MPC”. In: *IEEE Robotics and Automation Letters* 10.5 (May 2025).
- [10] Rel Guzman, Rafael Oliveira, and Fabio Ramos. “Bayesian Optimisation for Robust Model Predictive Control under Model Parameter Uncertainty”. In: *2022 International Conference on Robotics and Automation (ICRA)*. 2022 IEEE International Conference on Robotics and Automation (ICRA). Philadelphia, PA, USA: IEEE, May 23, 2022.
- [11] Jasper Snoek, Hugo Larochelle, and Ryan P. Adams. *Practical Bayesian Optimization of Machine Learning Algorithms*. Aug. 29, 2012.
- [12] Mahdi Nobar et al. “Guided Bayesian Optimization: Data-Efficient Controller Tuning With Digital Twin”. In: *IEEE Tran. on Automation Science and Engineering* 22 (2025).
- [13] Daniel Widmer et al. “Tuning Legged Locomotion Controllers via Safe Bayesian Optimization”. In: *Proceedings of The 7th Conference on Robot Learning*. Ed. by Jie Tan, Marc Toussaint, and Kourosh Darvish. Vol. 229. Proceedings of Machine Learning Research. PMLR, Nov. 6, 2023.
- [14] David Eriksson and Martin Jankowiak. “High-dimensional Bayesian optimization with sparse axis-aligned subspaces”. In: *Proceedings of the Thirty-Seventh Conference on Uncertainty in Artificial Intelligence*. Vol. 161. Proceedings of Machine Learning Research. PMLR, July 27, 2021.
- [15] David Eriksson and Matthias Poloczek. “Scalable Constrained Bayesian Optimization”. In: *Proceedings of The 24th International Conference on Artificial Intelligence and Statistics*. Ed. by Arindam Banerjee and Kenji Fukumizu. Vol. 130. Proceedings of Machine Learning Research. PMLR, Apr. 13, 2021.
- [16] Armand Jordana et al. “Force Feedback Model-Predictive Control via Online Estimation”. In: *2024 IEEE International Conference on Robotics and Automation (ICRA)*. Yokohama, Japan: IEEE, May 13, 2024.
- [17] Sebastien Kleff et al. “High-Frequency Nonlinear Model Predictive Control of a Manipulator”. In: *2021 IEEE International Conference on Robotics and Automation (ICRA)*. 2021 IEEE International Conference on Robotics and Automation (ICRA). Xi’an, China: IEEE, May 30, 2021.
- [18] David Mayne. “A Second-order Gradient Method for Determining Optimal Trajectories of Non-linear Discrete-time Systems”. In: *International booktitle of Control*. Vol. 3. Issue: 1. Jan. 1966.
- [19] Arne Wahrburg and Kim Listmann. “MPC-based admittance control for robotic manipulators”. In: *2016 IEEE 55th Conference on Decision and Control (CDC)*. Dec. 2016.
- [20] Topi Paananen et al. “Variable selection for Gaussian processes via sensitivity analysis of the posterior predictive distribution”. In: *Proceedings of the Twenty-Second International Conference on Artificial Intelligence and Statistics*. Ed. by Kamalika Chaudhuri and Masashi Sugiyama. Vol. 89. Proceedings of Machine Learning Research. PMLR, 2019.
- [21] Justin Carpentier et al. “The Pinocchio C++ library - A fast and flexible implementation of rigid body dynamics algorithms and their analytical derivatives”. In: *IEEE/SICE Int. Symposium on System Integration*. 2019.
- [22] Anders Prier Lindvig et al. “ur.rtdc: An Interface for Controlling Universal Robots (UR) using the Real-Time Data Exchange(RTDE)”. In: *2025 IEEE/SICE International Symposium on System Integration (SI)*. 2025, pp. 1118–1123.
- [23] Omotuyi O., Akinola I., and A. Saha. *Bridging the Sim-to-Real Gap for Industrial Robotic Assembly Applications Using NVIDIA Isaac Lab*. Nvidia technical report. 2023.
- [24] Maximilian Balandat et al. “BoTorch: A Framework for Efficient Monte-Carlo Bayesian Optimization”. In: *Advances in Neural Information Processing Systems* 33. 2020.
- [25] Miles Olson et al. “Ax: A Platform for Adaptive Experimentation”. In: *AutoML 2025 ABCD Track*. 2025.